physica **pss** status solidi a

www.pss-a.com

applications and materials science

The role of hydrogenation and gettering in enhancing the efficiency of next-generation Si solar cells: An industrial perspective

Feature Article

Brett Hallam[*,1], **Daniel Chen**[1], **Moonyong Kim**[1], **Bruno Stefani**[1,2], **Bram Hoex**[1], **Malcolm Abbott**[1], and **Stuart Wenham**[1]

[1] School of Photovoltaic and Renewable Energy Engineering, University of New South Wales, Anzac Parade, 2052 Sydney, Australia
[2] School of Engineering, Federal University of Rio, Grande do Sul, Porto Alegre, Brazil

* Corresponding author: e-mail brett.hallam@unsw.edu.au, Phone: +61 2 9385 0411, Fax: +61 2 9385 7762

We discuss the importance of gettering and hydrogenation for next-generation silicon solar cells in the context of industrial cell fabrication. Gettering and hydrogenation play a vital role for p-type cell technologies in improving the silicon material's minority charge carrier lifetime. These mechanisms are naturally incorporated during screen-printed cell fabrication through the phosphorus emitter diffusion, silicon nitride deposition and subsequent metallisation firing processes. While the transition towards emitters with lower dopant concentrations and/or thermal oxide passivation can reduce surface recombination, it can negatively impact the ability to getter common impurities such as iron. For cell technologies with alternative low-temperature metallisation approaches, the ability to hydrogenate bulk defects is greatly reduced. Ultra-high efficiency n-type technologies tend to use heterojunction structures rather than diffused layers, but in doing so, do not benefit from phosphorus gettering. Also, particularly for amorphous silicon-based heterojunction structures, the imposed temperature constraints strongly limit the ability to passivate bulk defects. As a result, high-efficiency n-type technologies rely on the use of 'high-quality' wafers or would require the deliberate addition of gettering and hydrogenation processes before cell fabrication. A potential high-efficiency hybrid homojunction/heterojunction structure is then discussed that could naturally enable gettering and bulk hydrogenation throughout cell fabrication.
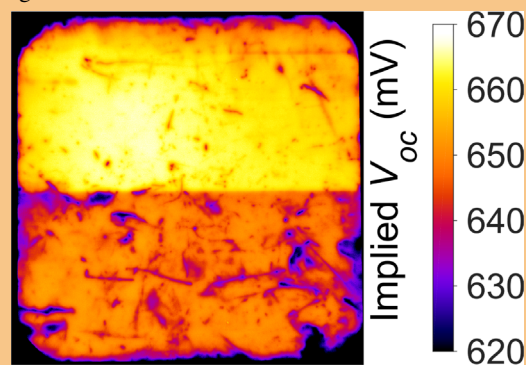
Calibrated implied open circuit voltage (V_{oc}) map of a p-type mono-crystalline wafer highlighting the impact of pre-hydrogenating the top half of the wafer.

1 Industrial silicon solar cells Silicon solar cell efficiencies are rapidly improving with record n-type and p-type devices are now 26.6 and 25.0%, respectively [1, 2]. Even p-type multi-crystalline solar cells now have efficiencies of up to 21.6% [3]. However, there is still significant debate if n-type or p-type silicon substrates should be utilised for the fabrication of future industrial silicon solar cells, even though p-type devices heavily dominate the market. In 2016, the estimated production capacity of crystalline silicon solar cells was approximately 70 GW [4], with n-type solar cells only accounting for 6–7% of cell production [4–6]. A trend towards n-type silicon solar cell manufacturing is often forecasted in roadmaps such as the International Technology Roadmap for PV (ITRPV).

For example, in the 2011 ITRPV, it was predicted that n-type solar cell technologies would have 35% of market share by 2016 [7]. However, the actual market share was still well below 10%. A lot of the hype about the use of n-type silicon substrates has been focussed on to the avoidance of boron-oxygen related light-induced, or more specifically, carrier-induced degradation (CID) which is present in p-type silicon [8]. Also, n-type materials have a lower sensitivity to recombination caused by transition metals such as interstitial iron (Fe_i) [9], and are consequently expected to have higher bulk minority carrier lifetimes. Another major driving force has been for differentiation in the market, particularly for new entrants [6, 10, 11]. However, current predictions by the ITRPV and Bloomberg New Energy Finance only have a predicted market share of 30–40% for n-type silicon by 2026 [4, 5]. Shorter-term predictions are also more modest, with estimates of a market share of 11–13% by 2018, while predictions from Solar Media suggest no increase in market share for n-type silicon in the same timeframe [6].

There are many good reasons why the domination of p-type silicon solar cells could continue well into the future. Firstly, the cell processing for p-type solar cells is inherently simple compared to that required for many n-type technologies. For example the use of proven and well-established processes such as self-cleaning $POCl_3$ tube furnace diffusions for emitter formation and screen-printed formation of the aluminium back-surface field (Al-BSF), in contrast to lengthy, high-temperature processes associated with boron-diffusions for n-type silicon wafers. This simplicity has resulted in the lowest cost silicon solar cells being fabricated on p-type multi-crystalline silicon substrates, with Trina's in-house module costs for the first quarter in 2016 of US$ 0.35/W_p [4].

Secondly, there has been a rapid progress of cell efficiencies for p-type devices on both mono-crystalline and multi-crystalline substrates in high-volume manufacturing. Peak solar cell efficiencies of 22.13% [12] and 21.63% [3] have been achieved on

Brett Hallam completed a Bachelor of Engineering degree in Photovoltaics and Solar Energy and Bachelor of Science in Physics, and Physical Oceanography/Meteorology at the University of New South Wales (UNSW), Sydney, Australia, in 2009, graduating with the University Medal. He then completed postgraduate studies at UNSW in Photovoltaic Engineering where he developed advanced hydrogenation and laser doping processes in 2014. He is now the Research Director for Advanced Hydrogenation at UNSW, focussing on the development of hydrogen passivation laser-based processes for silicon solar cell fabrication.

mono-crystalline and multi-crystalline substrates, respectively. This has been driven by the continuous development of new metallisation pastes, improved rear surface passivation from the implementation of a passivated emitter with rear local contact (PERC) structure, and advanced hydrogenation processes [3]. In addition, there were improvements in crystallisation with the development of 'high-performance' multi-crystalline silicon grown by seeded directional solidification [13]. Average industrial p-type cell efficiencies on production lines of leading manufacturers are now up to 21.6% for monocrystalline PERC solar cells [14] and 20.2% for multi-crystalline solar cells [15, 16]. Multiple other manufacturers are reporting average production efficiencies in excess of 21% [17, 18] and 20% [16, 19], respectively. In comparison, industrial n-type technologies have struggled to achieve significantly higher levels of performance, without going to more advanced solar cell architectures employing heterojunction structures [10, 11, 20–24]. The shift from the manufacturing of standard p-type Al-BSF cells to PERC solar cells is also a much smaller change to production than a swap to n-type technologies.

The simplicity, low-cost fabrication and progress of p-type solar cell technologies have seen surprising entrants into the p-type market including SunPower, who until recently was solely focused on high-efficiency n-type devices. However, through the acquisition of Cogenra, Sunpower has diversified to include the 'P-Series' module, based on p-type multi-crystalline silicon solar cell with a low-cost shingling approach. With this acquisition, Sunpower is expecting half of its future cell production to be based on p-type substrates [25].

Thirdly, the benefits of gettering and hydrogenation that naturally occur during p-type solar cell fabrication allow for an enhancement in the bulk minority carrier lifetime of the silicon. These processes can remove detrimental transition metallic impurities such as iron from the bulk of the silicon [26, 27]. They can also allow for the passivation of a range of structural [28–30], impurity related [26], process-induced [31, 32] and carrier-induced defects [33]. In contrast, many high-efficiency n-type technologies move away from processes that can enable gettering and hydrogenation of bulk silicon material, therefore requiring substrates with high initial bulk minority carrier lifetimes. While p-type devices are more susceptible from bulk lifetime degradation caused by iron, n-type devices are more sensitive to other metallic impurities such as copper, chromium and nickel [34]. There are also reports emerging of various degradation mechanisms in n-type devices such as carrier- [35] and potential-induced degradation [36], and instabilities in surface passivation [37]. The presence of such instabilities in n-type silicon, the impact of various metals, and the development of defect engineering methods to improve the quality of p-type silicon are removing several arguments for a potential shift towards n-type devices.

This paper will discuss the role of both of gettering and hydrogenation in enhancing the performance of silicon solar cells in the context of industrial solar cell fabrication.

1.1 Integrating gettering and hydrogenation into industrial silicon solar cell fabrication Gettering and hydrogenation are essential processes for the fabrication of high-efficiency industrial silicon solar cells. While this may seem obvious when fabricating solar cells on 'low-quality' substrates as reported in Ref. [26], it is perhaps less obvious as a necessity for the fabrication of solar cells using 'high-quality' silicon substrates with multi-millisecond bulk lifetimes. Often, high-efficiency solar cell architectures rely on the use of silicon substrates with high initial bulk lifetimes and perform minimal processing on the samples to avoid a potential degradation of the bulk silicon material properties throughout the fabrication [38], rather than deliberately using defect engineering methods such as gettering and hydrogenation. However, incorporating these methods should be seen as an opportunity to improve the electronic quality of silicon material throughout the fabrication sequence, hence reducing the impact of bulk recombination. Doing so could be considered as a pathway to (i) improve cell efficiencies and (ii) reduce cost through either an improvement in cell efficiency or a relaxation of the initial silicon material quality requirements. For example, recent work has demonstrated that n-type silicon can significantly benefit from bulk hydrogenation, with increases the τ_{bulk} of 'low quality' commercial grade n-type wafers from $90\,\mu s$ to $3.4\,ms$, suggesting that such wafers could be compatible with the fabrication of 24% efficient solar cells [32].

A significant benefit of using both gettering and hydrogenation is that they are complementary methods for defect engineering. Firstly, gettering can remove impurities from the bulk of the silicon, and hydrogenation can subsequently be used to passivate the remaining impurities. The combined approach is particularly important for multi-crystalline silicon, whereby impurity-decorated structural defects are more of a challenge to hydrogenate [39]. Therefore, gettering can be used to remove impurities from structural defect sites in the bulk of the silicon to make the defects more responsive to subsequent hydrogen passivation treatments. Where possible, the processes should be integrated into the solar cell fabrication sequence without adding processing steps. Therefore, the processes should simultaneously enable device structure formation.

2 Gettering and hydrogenation in conventional industrial Al-BSF silicon solar cell The conventional screen-printed solar cell with a full area Al-BSF is still the dominant industrial silicon solar cell technology, with a market share of 89% [4]. This technology is a great example whereby the processes used throughout the fabrication sequence can simultaneously enable device structure formation and perform defect engineering to improve the

bulk lifetime of the silicon. The typical fabrication sequence for a standard industrial silicon solar cell with a full area Al-BSF is shown in Fig. 1.

2.1 Gettering in full-area Al-BSF solar cells The processes of key importance to gettering in conventional Al-BSF solar cells are the POCl$_3$ emitter diffusion for the formation of the p–n junction and the co-firing process for the formation of the Al-BSF. The use of the screen-printed contacts typically requires a surface dopant phosphorus concentration of more than 1×10^{20} atoms/cm^3 to enable ohmic contact to the silicon and sufficient shielding from minority carrier recombination at the metal/silicon interface. For the conventional screen-print emitter diffusion, the POCl$_3$ diffusion often results in the presence of inactive phosphorus atoms near the surface of the silicon. This inactive phosphorus can generate defects and silicon phosphate (SiP) precipitates that act as gettering sites for metallic impurities [40–44]. Hence, while this 'dead layer' can increase recombination within the emitter, it acts as an efficient gettering site. The subsequent wet chemical process for edge junction isolation can also indirectly contribute towards gettering through the removal of the emitter on the rear of the device. In addition to eliminating the conductive shunt path between the front and rear contact, any impurities gettered to the rear phosphorus diffused layer are etched off during this process, and therefore removed from the device. This ensures that impurities gettered to the rear or the device cannot be re-injected back into the bulk during subsequent high-temperature processing.

The co-firing process can also potentially enable gettering. During the formation of the Al-BSF, a molten Al/Si layer is present over the entire rear surface of the device. There are various reports of gettering for impurities using the Al/Si eutectic in a segregation-related effect, whereby metals have a higher solubility in the molten Al/Si layer than that in solid silicon [45–47]. However, for the short time scales involved in the co-firing process, this is
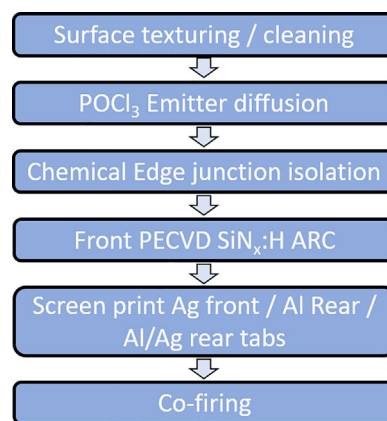


```
┌─────────────────────────────────┐
│   Surface texturing / cleaning  │
└─────────────────────────────────┘
                 ⬇
┌─────────────────────────────────┐
│      POCl₃ Emitter diffusion    │
└─────────────────────────────────┘
                 ⬇
┌─────────────────────────────────┐
│  Chemical Edge junction isolation│
└─────────────────────────────────┘
                 ⬇
┌─────────────────────────────────┐
│     Front PECVD SiNₓ:H ARC      │
└─────────────────────────────────┘
                 ⬇
┌─────────────────────────────────┐
│ Screen print Ag front / Al Rear /│
│          Al/Ag rear tabs        │
└─────────────────────────────────┘
                 ⬇
┌─────────────────────────────────┐
│            Co-firing            │
└─────────────────────────────────┘
```

Figure 1 Process flow for the fabrication of conventional industrial screen-printed solar cells with a full area aluminium back surface field (Al-BSF).

assumed to be a negligible effect for impurities such as iron [48]. On the other hand, the high temperatures used for the rapid co-firing process (typically in the vicinity of 700–800 °C) can result in a potential 'poisoning' of the bulk silicon material through the release of impurities from gettered sites in the phosphorus emitter and the dissolution of iron precipitate sites [49–52].

To illustrate the impact of a typical screen-print compatible emitter diffusion and co-firing, test samples were fabricated on $1.6\,\Omega.\text{cm}$ p-type boron-doped Czochralski (Cz) grown silicon substrates. Wafers were textured and then $POCl_3$ diffused to a sheet resistance of $60\,\Omega/\square$ with an active phosphorus surface concentration of $4 \times 10^{20}/\text{cm}^3$ (see the red profile in Fig. 4 for the diffusion profile). Control samples were left non-diffused. After the subsequent PSG removal, a 75 nm layer SiN_x:H with a refractive index of 2.08 was deposited on both surfaces using a Roth & Rau MAiA plasma-enhanced chemical vapour deposition (PECVD) system. Fast firing was performed with a peak measured sample temperature of 740 °C. The effective minority carrier lifetime of the wafers was monitored using the quasi-steady-state photoconductance (QSS-PC) method [53] on a Sinton Instruments WCT-120 tool using the generalised analysis [54]. $[Fe_i]$ concentrations were extracted using the known method [55] before and after a 10 s exposure to illumination. It should be noted that for these symmetrical lifetime samples, the potential gettering of iron by aluminium was not investigated.

On wafers with a background Fe_i concentration of $[Fe_i] = 2.8 \times 10^{11} \pm 1.7 \times 10^{11}/\text{cm}^3$, before firing this conventional screen-printed diffusion reduced $[Fe_i]$ to $<2.1 \times 10^{10} \pm 3.0 \times 10^9/\text{cm}^3$ (see Table 1). This resulted in an improvement of iron-boron (Fe_i-B) related bulk lifetime ($\tau_{\text{bulk, Fe-B}}$) limitation at an excess minority carrier concentration of $\Delta n = 0.1 \times N_a$ from $22.3 \pm 0.7\,\mu\text{s}$ to $105.9 \pm 0.6\,\mu\text{s}$. After firing, a slight reduction in $[Fe_i]$ was observed on non-diffused samples (to values of $1.4 \times 10^{11} \pm 1.1 \times 10^{11}/\text{cm}^3$), which may be due to a gettering or precipitation-related effect. However, for diffused samples with much lower initial $[Fe_i]$ values of $5.4 \times 10^9 \pm 1.1 \times 10^9/\text{cm}^3$, the firing process caused a net increase of $[Fe_i]$ to values of $2.1 \times 10^{10} \pm 3.0 \times 10^9/\text{cm}^3$, indicating a poisoning of the bulk. Despite the increase in $[Fe_i]$ after firing, the samples displayed increased bulk lifetimes (from $105.9 \pm 0.6\,\mu\text{s}$ to $131.4 \pm 2.4\,\mu\text{s}$ on the

diffused samples), which can be attributed to the simultaneous hydrogenation of the bulk.

2.2 Hydrogenation in full area Al-BSF solar cells
The processes of key importance to hydrogenation are the PECVD of hydrogenated silicon nitride (SiN_x:H) and the co-firing process. For the deposition of SiN_x:H, the plasma process itself can act as a hydrogenation process through the generation of hydrogen radicals from silane (SiH_4) and ammonia (NH_3) which are the most commonly used precursors. However, the temperatures in the vicinity of 400 °C used during the deposition limits the diffusion of hydrogen through the emitter layer, where almost all the hydrogen is in a low-mobility negative charge state (H^-) [56, 57]. For example, in phosphorus-doped silicon with a doping density of $1 \times 10^{20}/\text{cm}^3$, assuming Sah–Shockley occupation statistics [58, 59], the thermal generation of the highly mobile neutral hydrogen charge state (H^0), is expected to be only 0.001%, and even less for more heavily phosphorus-doped silicon.

However, hydrogen is also incorporated into the SiN_x layer and can later be released during subsequent thermal processing. The implementation of PECVD SiN_x:H was seen as a vital development for multi-crystalline silicon solar cells, with hydrogen passivation leading to performance enhancements of 15% relative [28]. The metallisation co-firing process acts to release hydrogen from the SiN_x:H layer [60], and enables the diffusion of atomic hydrogen through the emitter layer, into the bulk silicon material. The higher temperatures during the firing process increase the diffusivity of each of the hydrogen charge states, as well increasing the concentration of neutrally charged hydrogen (H^0) as the silicon becomes more intrinsic [61]. At a temperature of 700 °C, the thermally generated fractional H^0 concentration is increased by two orders of magnitude compared to that at 400 °C. The co-firing process can greatly improve the effective lifetime of the material through the passivation of bulk and surface-related defects.

Symmetrical test structures were fabricated on boron-doped multi-crystalline and mono-crystalline wafers. Wafers were diffused, passivated with PECVD SiN_x:H and fired as previously described (peak measured sample temperature of 740 °C). Figure 2 shows example 1-sun calibrated implied V_{oc} maps [62] obtained on multi-crystalline silicon wafers from photoluminescence (PL) imaging [63], before and after a typical co-firing process. The PL images were post-processed for point-spread-function deconvolution [64, 65]. The images indicate that the deposition of PECVD SiN_x:H was ineffective at passivating grain boundaries (see Fig. 2a). However, the absence of recombination activity in these regions in Fig. 2b suggests that the defects were readily passivated during the co-firing process. The images highlight a substantial improvement in all areas of the wafer, including the heavily dislocated regions. For the monocrystalline wafers, the firing process caused an increase in the bulk

Table 1 Interstitial iron concentration ($[Fe_i]$) before and after a standard co-firing process on non-diffused samples and samples with an emitter suitable for screen-printed contacts.

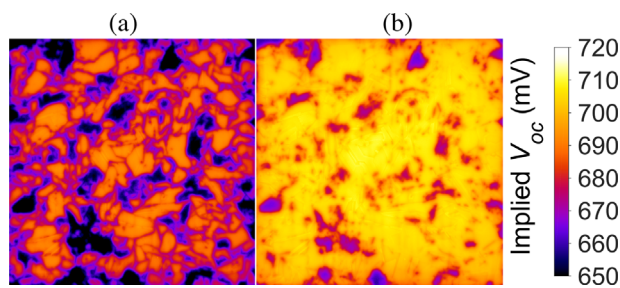|	before firing (/cm³)	after firing (/cm³)
without diffusion	$2.8 \times 10^{11} \pm 1.7 \times 10^{11}$	$1.4 \times 10^{11} \pm 1.1 \times 10^{11}$
screen-print diffusion	$5.4 \times 10^9 \pm 1.1 \times 10^9$	$2.1 \times 10^{10} \pm 3.0 \times 10^9$

(a)   (b)

Figure 2 Calibrated 1-sun implied V_{oc} maps of a diffused multi-crystalline silicon wafer (a) after the deposition of PECVD SiN$_x$:H, and (b) after the subsequent firing process (peak measured sample temperature of 740 °C).

lifetime from $105.9 \pm 0.6\,\mu s$ to $131.4 \pm 2.4\,\mu s$, as well as a reduction in the emitter dark saturation current density (J_{0E}) from $97.6 \pm 1.1\,\text{fA cm}^{-2}$ down to $81.7 \pm 1.4\,\text{fA cm}^{-2}$ (per side).

Although a certain level of hydrogen passivation can be achieved during a conventional co-firing process, the process is not effective for the passivation of a variety of defects such as carrier-induced defects. Nonetheless, the use of SiN$_x$:H and a co-firing process can enable the passivation of additional defects when further hydrogenation processes are performed on the finished device. For example, recent progress in advanced illuminated hydrogenation techniques has seen the development of sub ten second processes to completely eliminate boron-oxygen-related CID on finished industrial solar cells [66, 67]. This has resulted in the development of a new generation of industrial tools for CID mitigation, and a reduced concern from solar cell manufacturers in relation to the boron-oxygen defect. Other defects in multi-crystalline silicon such as dislocation clusters also respond well to advanced hydrogenation processes [66, 68]. While such illuminated hydrogenation processes may be performed as a separate processing step, they can potentially be integrated into the cool-down section of the co-firing process.

3 Gettering and hydrogenation in high-efficiency p-type PERC screen-printed silicon solar cells The transition of the PV industry to PERC solar cells can have significant implications for gettering and hydrogenation. The structural difference for PERC solar cells compared to conventional full area Al-BSF cells is the inclusion of rear surface passivation layers and the localised formation of Al-BSF regions. From a process point of view, this requires the addition of deposition processes for rear dielectric layer(s) and a laser-based process for forming localised openings in the rear surface dielectric stack. A typical process flow for the PERC solar cell using a rear surface passivation stack of PECVD AlO$_x$:H/SiN$_x$:H is shown in Fig. 3.

3.1 Gettering in PERC solar cells For gettering, the continued use of a POCl$_3$ diffused emitter still enables phosphorus gettering. However, several aspects of moving
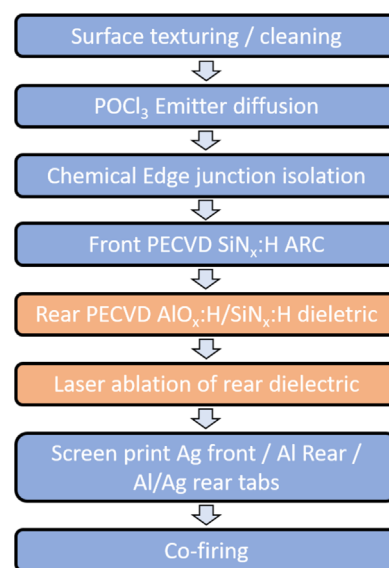

Figure 3 Process flow for the fabrication of industrial screen-printed PERC solar cells with rear surface passivation achieved using a stack of PECVD AlO$_x$:H and SiN$_x$:H.

towards the use of high-efficiency emitters with low J_{0E} values can affect the ability to getter impurities throughout the fabrication sequence effectively. A key aspect of producing high-efficiency emitters is the avoidance of a 'dead layer' that can reduce the short circuit current of the device. Silver screen-printing pastes have typically limited the ability to use lightly doped emitters. Traditional pastes required high surface dopant concentrations for adequate contact resistance and effective shielding from minority carrier recombination at the metal/Si interface [69]. However, newly developed pastes have reduced contact resistivity by a factor of 10–1000 with effective shielding of minority carriers [69], enabling more lightly doped emitters to be used for screen-printed solar cells. The elimination of inactive phosphorus can reduce Auger and Shockley–Read–Hall recombination in the emitter, leading to reduced J_{0E} values. However, the reduction of inactive- and total phosphorus concentrations in the emitter layer can also reduce the effectiveness of gettering [44].

An alternative method for fabricating high-efficiency emitters is through the use of a selective emitter structure. Selective emitter structures have lightly diffused regions underneath the passivated regions, and only use heavily doped regions underneath the metal contacts. Selective emitter structures overcome potential issues with recombination at the metal/Si interface and are compatible with regular screen-printed contacts. One approach for fabricating a selective emitter with screen-printed contacts is to form a heavily diffused emitter over the entire surface, followed by patterned deposition e.g. by screen-printing of a masking layer in the regions that will later form the metal contacts. Subsequently, the exposed regions are chemically etched to remove the heavily diffused region, leaving a lighter diffused region that will later form the passivated

emitter regions. After the deposition of the PECVD SiNₓ:H layer, screen printed contacts are aligned to the heavily doped regions [70]. In this approach, the use of a heavy diffusion can enable a more effective gettering of impurities, followed by the removal of the impurities from the device structure during the chemical etch process. The chemical removal of such impurities eliminates a potential release of impurities from precipitate sites during co-firing from gettered sites back into the bulk of the silicon.

The use of an emitter etch-back is also applicable for homogenous emitter designs. An emitter etch-back process can be realised during the chemical edge junction isolation process, using either a wet-chemical [71] or a gas-phase etch [72]. Industrial tools such as the Kuttler wet-chemical edge junction isolation baths have a gas-phase etch back process incorporated from the vapours of the strong chemicals that are used to remove the rear emitter completely and planarise the rear surface. This tool and gas-phase etch back process were used to fabricate industrial p-type PERC solar cell with efficiencies over 20% [73]. Alternatively, a heavy gettering diffusion process can be performed on the wafer, followed by the complete removal of the diffusion in an etching process. Subsequently, the wafers can be re-diffused to form the desired emitter. However, this adds extra processing steps and significantly increases the thermal budget and costs for the device.

Another process modification to reduce front surface recombination is the use of thermal silicon dioxide (SiO₂) surface passivation. The use of SiO₂ passivation significantly reduces the interface defect state density, particularly when coupled with hydrogen passivation [74]. Such approaches have been used for the fabrication of world record Passivated Emitter, and Rear Locally diffused (PERL) solar cells [2, 75]. When this approach is used on the front surface of industrial silicon solar cells, the thickness of the SiO₂ layer is typically in the vicinity of 10–20 nm and capped by PECVD SiNₓ:H for antireflection purposes [76, 77]. In addition to passivating the silicon surface, the thermal oxidation process significantly changes the diffusion profile as the thermal process redistributes the phosphorus dopants and consumes silicon from the substrate, leading to further reductions in the surface dopant concentration. While this structure provides low J_{0E} values in the passivated region, it can result in poisoning of the silicon from the re-injection of gettered impurities in the emitter layer as well as the release of iron from precipitate sites. This is particularly the case when the oxidation process is performed at a higher temperature than that used for the diffusion process [49]. Hence, preferably, impurity-decorated gettering sites should be removed from the device before the thermal oxidation process.

To highlight the impact of shifting towards the use of a lighter emitter diffusion and an oxidation process on gettering, symmetrical lifetime test samples were fabricated on 1.6 Ω.cm p-type boron-doped Cz wafers. Selected samples received a gettering diffusion process (30 Ω/□) followed by a complete removal of the diffused layers. Two separate diffusion processes were used: (i) a screen-print (SP) diffusion process with a sheet resistance of 60 Ω/□ and (ii) a lightly doped emitter (LDE) with a sheet resistance of 110 Ω/□. After the subsequent process, selected samples had a thin thermal oxide grown at 890 °C for 10 min. The oxidation process resulted in a slight increase of the sheet resistance of the emitters, to values of 65 and 130 Ω/□, respectively. The electrically active phosphorus dopant concentrations for the four diffusion profiles were measured using electrochemical capacitance-voltage (ECV) measurements (see Fig. 4). The graph highlights a reduced surface dopant concentration and shallower diffusion profile for the lightly doped emitter (2.4×10^{20}/cm³) compared to that of the screen-print emitter (3.7×10^{20}/cm³). Furthermore, the oxidation process led to substantial reductions in the peak surface concentration of phosphorus dopants for the SP and LDE diffusion down to 2.5×10^{19}/cm³ and 5.8×10^{19}/cm³, respectively. The oxidation also leady to a substantial increase in junction depth, particularly for the LDE diffusion. After the oxidation process, the SP diffusion was no longer suitable for use with screen-printed contacts, with a phosphorus surface dopant concentration that is too low to enable effective contact. To avoid such severe modifications to the doping profile, a lower temperature can be used during thermal oxidation, while still receiving the benefits of improved surface passivation.

The use of an LDE reduced the ability to getter iron. As shown in Fig. 5, before firing, samples with the LDE had [Fe$_i$] of up to $1.0 \times 10^{10} \pm 1.3 \times 10^{9}$/cm³ (compared to values of [Fe$_i$] $5.4 \times 10^{9} \pm 1.1 \times 10^{9}$/cm³ for the SP emitter). The oxidation process caused a substantial increase in [Fe$_i$] for both the SP and LDE emitters, with resultant [Fe$_i$] of $2.9 \times 10^{10} \pm 3.3 \times 10^{9}$/cm³ and $4.5 \times 10^{10} \pm 5.5 \times 10^{9}$/cm³, respectively. After firing, the [Fe$_i$] on all diffused samples increased. The SP diffusion without a thermal oxidation process had the lowest [Fe$_i$] with values
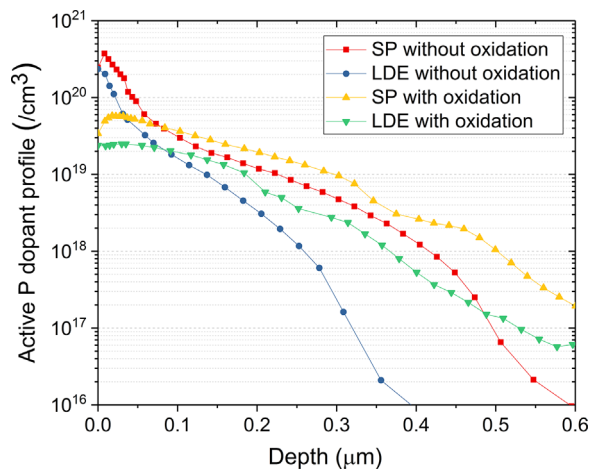

Figure 4 Electrically active phosphorus doping profiles from electrochemical capacitance-voltage (ECV) measurements for screen-print (SP) and lightly doped emitters (LDE), with and without a subsequent thermal oxidation.
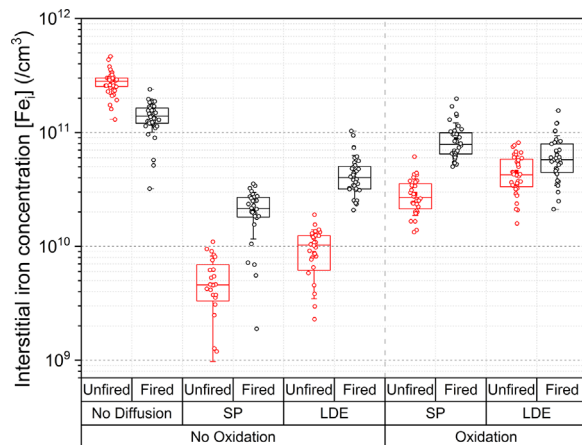
Figure 5 Interstitial iron concentrations ($[Fe_i]$) before and after firing of non-difused samples, as well as diffused samples with either a screen-print (SP) or light-doped emitter (LDE) diffusion, with and without a thermal oxidation process.

$2.1 \times 10^{10} \pm 3.0 \times 10^{9}/cm^3$. The LDE diffusion without an oxidation process had an $[Fe_i]$ of $4.4 \times 10^{10} \pm 6.0 \times 10^{9}/cm^3$ and the oxidised SP and LDE diffusions showed higher average $[Fe_i]$ in the range of $8.8 \times 10^{10} \pm 1.1 \times 10^{10}/cm^3$ and $6.1 \times 10^{10} \pm 1.0 \times 10^{10}/cm^3$, respectively. Although the oxidation process caused an increase in $[Fe_i]$, the final values were still lower than the inherent $[Fe_i]$ in the non-diffused wafers after firing. This clearly demonstrates the benefits that performing even a light phosphorus diffusion throughout the cell fabrication sequence can have for gettering impurities such as iron. A heavy pre-gettering step can also be performed before device fabrication to improve the effectiveness of gettering impurities such as iron. In this instance, applying such a pre-gettering step reduced the $[Fe_i]$ on SP and LDE emitters without thermal oxidation to below the detection limit, while for the SP and LDE diffusions with thermal oxidation, the $[Fe_i]$ values were $7.8 \times 10^{9} \pm 1.7 \times 10^{9}/cm^3$ and $1.1 \times 10^{10} \pm 2.3 \times 10^{9}/cm^3$, respectively. However, this approach adds processing steps and would generally not be considered viable for industrial cell production.

The different diffusion and oxidation processes also had a significant impact on the τ_{bulk} of the silicon material. Table 2 shows the corresponding τ_{bulk} extracted at an injection level of $\Delta n = 9.1 \times 10^{14}/cm^3$ after removal of Auger, radiative and J_{0E} (determined at $\Delta n = 1.0 \times 10^{16}/cm^3$) related lifetime components [78, 79]. The image highlights the poor inherent quality of the material with $\tau_{bulk} < 25\,\mu s$ before firing. All diffusion/oxidation processes resulted in an improvement in bulk lifetime, resulting in $\tau_{bulk} > 100\,\mu s$ for all diffusion processes. These increases indicate a significant improvement in the bulk quality of the silicon material from the gettering of iron and/or other impurities, or other thermally related effects. The application of a pre-gettering process led to significant further enhancements of the τ_{bulk}, with the LDE diffusion performing better than the SP diffusion (see Fig. 6).

Table 2 Average bulk lifetime (τ_{bulk}) extracted at an excess carrier concentration of $\Delta n = 9.1 \times 10^{14}/cm^3$, and emitter saturation current density (J_{0E}) extracted at an excess carrier concentration of $\Delta n = 1.0 \times 10^{16}/cm^3$ on samples with and without various diffusion processes and oxidation. All values shown are before firing.

	τ_{bulk} (μs)	J_{0E} (fA cm^{-2})
no diffusion	22.3 ± 0.7	115.1 ± 2.3
SP	105.9 ± 0.6	97.6 ± 1.1
LDE	145.5 ± 1.5	61.6 ± 1.4
SP + oxidation	137.9 ± 2.8	56.6 ± 1.3
LDE + oxidation	163.9 ± 8.2	21.0 ± 0.5

Thermal oxidations also improved the τ_{bulk} of the silicon for both diffusions, with values of $380 \pm 20\,\mu s$ observed for the samples with an LDE diffusion and thermal oxidation.

In addition to the benefits to the τ_{bulk} that can occur through the use of high-efficiency emitter structures, substantially reduced J_{0E} values can be achieved. As shown in Table 2, the LDE diffusion had a substantially lower J_{0E} value ($61.6 \pm 1.4\,fA\,cm^{-2}$), compared to that of the SP diffusion ($97.6 \pm 1.1\,fA\,cm^{-2}$), due to a lower contribution from Auger recombination in the emitter. The application of a thermal oxidation process led to further reductions in the J_{0E} for both the SP and LDE diffusions, to values of 56.6 ± 1.3 and $21.0 \pm 0.5\,fA\,cm^{-2}$, respectively, due to further reductions in Auger related J_{0E} recombination and a reduced surface recombination velocity.

The transition to the use of a localised Al-BSF may also further reduce the ability to getter impurities during the co-firing process. Without a full area Al-BSF, a lateral transport of impurities is required to reach the localised molten Al/Si region, reducing the probability of gettering. However, this area requires further investigation.

3.2 Hydrogenation in PERC solar cells The addition of hydrogen-containing dielectric layers on the rear surface of PERC solar cells naturally leads to a higher concentration of hydrogen in the silicon bulk. This increases the passivation rates for defects such as the boron-oxygen complex [80]. This may be further enhanced by the used of lighter diffusions that more readily allow the diffusion of hydrogen into the bulk of the device through an increased generation of H^0. Also, the improved rear surface design results in higher carrier concentrations in the material. This has important implications for hydrogen passivation reactions requiring the injection of minority carriers for manipulating hydrogen charge state concentrations. The increased lifetimes in the material can increase the concentrations of the minority hydrogen charge species, therefore improving the response of the solar cell to the illuminated hydrogenation process. For CID-based mechanisms, the additional carriers generated for a given illumination intensity can also accelerate defect formation, which also assists with the mitigation process [81, 82].
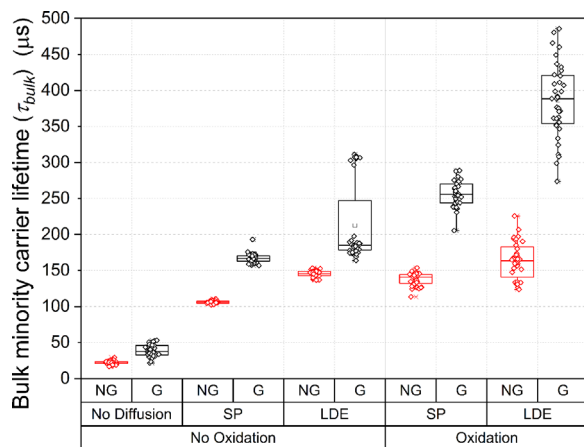
Figure 6 Bulk lifetime (τ_{bulk}) extracted at an excess carrier concentration of $\Delta n = 9.1 \times 10^{14}/cm^3$, on non-pre-gettered (NG) and pre-gettered (G) wafers, which are either non-diffused, have a screen-print (SP) diffusion or a lightly diffused emitter (LDE). Values are shown before firing.

For the non-gettered samples detailed in the previous section, firing led to substantial improvements in the J_{0E} for all diffusions (see Fig. 7a) through hydrogen passivation of defects and the Si/SiO$_2$ interface. For the LDE diffusion with thermal oxidation, J_{0E} values as low as 14.2 ± 0.6 fA cm^{-2} were obtained. For the conventional SP diffusion without thermal oxidation, J_{0E} values of 81.7 ± 1.5 fA cm^{-2} were obtained. In contrast, firing had a mixed impact on τ_{bulk} for the different groups (see Fig. 7b). For diffused samples without a thermal oxidation, the τ_{bulk} increased after firing, while for diffusions with thermal oxidations, the τ_{bulk} reduced slightly. Despite these slight reductions, the firing process is essential to enable a subsequent passivation of boron-oxygen defects.

However, hydrogen should not be thought of as purely beneficial for solar cells. Hydrogen can also be involved in the formation of recombination active defects in silicon solar cells. For example, recent reports of hydrogen-oxygen complexes in n-type silicon [83]. For the recently observed CID mechanism in multi-crystalline silicon [84], the extent of degradation has been observed to be modulated by changes to the dielectric layers [85] and firing conditions [86–89]. Multiple authors have eluded to a possibility of hydrogen being involved in the defect [86, 89–91] which could explain the increased severity of CID in multi-crystalline PERC solar cells compared to that in Al-BSF solar cells [84]. Another possible reason is the reduced J_0 values in high-efficiency solar cell architectures.

4 Gettering and hydrogenation in high-efficiency n-type technologies
The use of gettering and hydrogen passivation in commercial high-efficiency n-type silicon solar cells is more difficult to ascertain due to the commercial sensitivity of processes used by companies. Both gettering and hydrogenation can play an important role for such technologies, however, this is often not discussed in the literature.
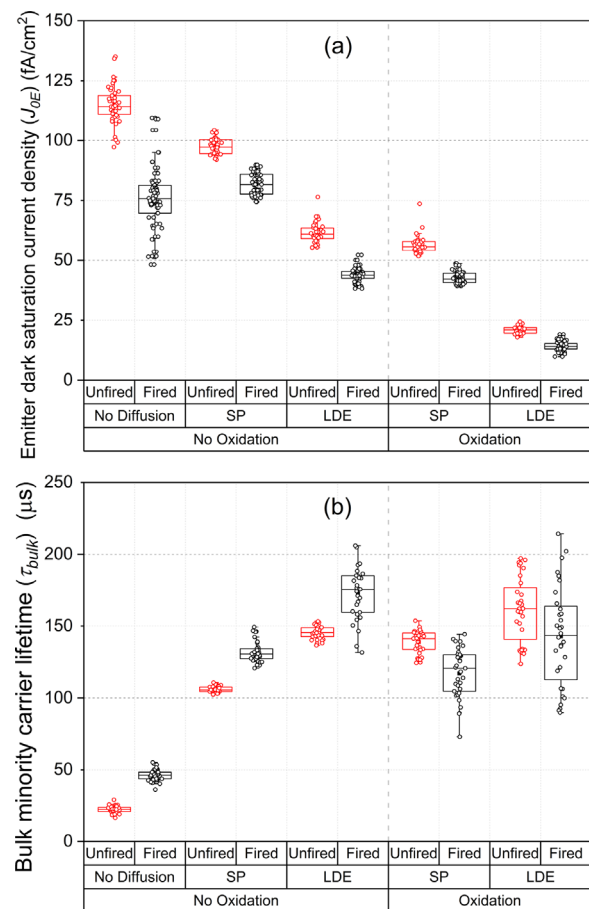

Figure 7 (a) Emitter dark saturation current density (J_{0E}) of non-gettered wafers that were non-diffused, have screen-print (SP) diffusion or lightly diffused emitter (LDE), with and without a thermal oxidation. Part (b) shows the corresponding bulk lifetime (τ_{bulk}) extracted at $\Delta n = 9.1 \times 10^{14}/cm^3$.

Furthermore, in general, the high-efficiency n-type solar cell technologies move away from a structure that enables a natural gettering and hydrogenation of the bulk material during cell fabrication. For such technologies, the use of hydrogen passivation is typically only discussed in the context of surface passivation. As an example, several papers and patents relating to the development of high-efficiency solar cells by Sanyo, Sunpower, Silevo and Tetrasun have eluded to the use of hydrogen-containing dielectric layers and/or subsequent processing in forming gas ambient [11, 92–96]. However, there was no mention of bulk defect passivation in those publications.

4.1 Gettering for screen-printed n-type technologies
Conventional screen-printed metallisation techniques require high-temperature firing processing to penetrate through surface dielectrics and/or form localised heavily doped regions to form electrical contacts. For solar cells structures that form boron- and phosphorus-doped regions before metallisation, the screen-printing is only required to establish electrical contact to the diffused

regions [21, 97]. The use of PECVD SiN$_x$:H and high firing temperatures for screen-printed n-type solar cells naturally enables the benefit of bulk hydrogenation. However, the advantages of bulk hydrogenation are often not discussed in the literature (e.g. see Refs. [21, 97]). Typically, the cells also feature a phosphorus diffusion either by POCl$_3$ diffusion [97] or ion implantation [21], which can also enable gettering [98, 99]. Again, the benefits of gettering are often not discussed. However, one example highlighting the importance and benefits of gettering for high-efficiency n-type solar cells was presented by Li et al. [97] from Trina Solar. For the rear interdigitated contact structure, the phosphorus diffusion process required to form the localised BSF was simultaneously used to form a heavily diffused region on the front surface for gettering purposes. This front surface diffusion was later removed by a chemical etch, and a light phosphorus diffusion was used to form the front surface field (FSF). The addition of this gettering process resulted in an efficiency enhancement of 0.2% absolute, to yield average efficiencies of 23.0% [97]. Those results clearly highlight the importance of defect engineering methods for high-efficiency device fabrication, and how such methods can be integrated into the process sequence while simultaneously enabling the formation of the device structure.

4.2 Hydrogenation for n-type solar cells with alternative metallisation technologies When metallisation technologies other than screen-printing are used, the need for high-temperature processing after dielectric deposition for the purpose of forming the device structure is often eliminated. Example metallisation technologies include sputtering or evaporation of aluminium, and plating [100]. For such metallisation schemes, laser-based processes including dielectric ablation and/or laser doping may be used to open the dielectric layers for contact definition [100]. Especially when using aluminium-based metallisation on diffused regions, temperatures should be kept below the Al/Si eutectic temperature of 577 °C. This avoids melting the diffused region, and a deterioration of the superior doping profiles for the purpose of field-effect passivation that can be realised by diffusion-based processes compared to that of Al/Si alloyed regions. However, this necessary avoidance of high-temperature processing after metal deposition limits the ability to passivate bulk defects in the device. Often, SiN$_x$:H layers require a high firing temperature to enable effective release of hydrogen and the diffusion of hydrogen into, and throughout the bulk of the device to enable passivation [101, 102], as was shown in Fig. 3. However, an improved level of bulk hydrogenation can be achieved by simply performing a high-temperature firing process directly after dielectric deposition and before the deposition of metal layers [103]. While forming gas annealing is a common method for fabricating high-efficiency solar cells [75, 104], rapid belt furnace annealing processes utilising hydrogen already existing in the device structure offer a more suitable solution for hydrogenation of

the bulk [103]. Such processing can be used for the passivation of surface-related and laser-induced defects [31]. The rapid process can also avoid a deterioration of bulk lifetime that can occur with extended annealing in the vicinity of 300–500 °C, which may be due to the nucleation of oxygen precipitate sites [103, 105]. A key contributor to the improved surface passivation includes the injection of minority carriers from the infrared lamps and rapid cooling during belt-furnace processes [106]. Such processes have been used to fabricate record n-type Passivated Emitter, Rear Totally diffused solar cells at 22.5% [107].

4.3 Hydrogenation and gettering for heterojunction solar cells Heterojunction solar cells with amorphous silicon (a-Si) based surface passivation layers currently hold the world record for silicon solar cell efficiencies at 26.6% (Kaneka) [1]. The pioneering work on this approach was conducted by Sanyo [108]. One strength of a-Si based heterojunction technologies is the excellent surface passivation provided by hydrogenated a-Si layers, through hydrogen passivation of defects at the interface and field-effect passivation by band bending [95]. The use of a heterojunction (or 'passivated contact') structure avoids Auger-related J_{0E} components associated with diffused emitter regions [109], leading to improved open circuit voltage capabilities. Another attributed strength is the low-temperature processing (typically with all steps performed below 200 °C) which prevents a degradation of the bulk minority carrier lifetime that may occur with high-temperature processing of low-quality silicon [38]. The process sequence for the fabrication of bifacial a-Si-based heterojunction solar cells is shown in Fig. 8.

However, the exclusive use of low process temperatures to fabricate the device structure can also be seen as a weakness of the technology. The processes used for forming the device structure do not enable gettering or hydrogenation for the bulk, and therefore do not allow for a potential improvement in the τ_{bulk} of silicon throughout the fabrication sequence. As a result, a-Si-based heterojunction devices are fabricated on 'high-lifetime' n-type Cz-grown or float zone (FZ) silicon. The absence of a phosphorus diffusion process during cell fabrication removes the ability to getter impurities from the bulk using conventional methods. To enable gettering of the bulk, a deliberate gettering process must be added (such as a heavy POCl$_3$-based phosphorus diffusion), followed by the complete removal of the diffused layer, before the device structure can be fabricated. This obviously adds processing steps and cost to the production sequence. Alternatively, recent work has demonstrated the ability to getter iron into dielectric layers such as SiN$_x$:H with prolonged annealing [110].

Heterojunction solar cells based on a-Si passivation also suffer from an incompatibility with hydrogenation of bulk defects. For example, at 150 °C, the diffusion coefficient of the dominant hydrogen charge species in p-type silicon in thermal equilibrium (H$^+$) is only 6×10^{-13} cm^2 s^{-1} [57]. Hence, it would take ~6.3 years to have a diffusion length of
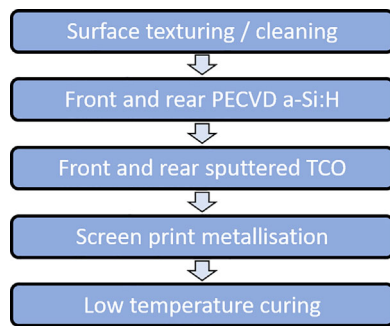
Figure 8 Process flow for the fabrication of bifacial a-Si-based heterojunction solar cells.

$100 \, \mu m$ required to distribute hydrogen throughout the device, which is clearly unfeasible for photovoltaic manufacturing. In n-type devices, for the dominant charge species (H^-), it would take $\sim 140 \, h$. Even using carrier injection to generate the highly mobile neutral charge species in either n-type or p-type silicon (H^0) would still require $\sim 3 \, h$. Another weakness of a-Si-based surface passivation is that annealing at temperatures $>250 \, °C$ after the a-Si deposition typically leads to a deterioration of surface passivation due to the dehydrogenation of the a-Si layers [111]. This excludes the possibility of a subsequent introduction of hydrogen into the device at higher temperatures. Consequently, a deliberate prior introduction of hydrogen into the device and distribution throughout the device would be required, before the a-Si deposition takes place, to enable bulk defect passivation. This would again require additional processing steps.

It is a similar story for heterojunction solar cells using tunnelling oxide layers in regards to gettering and hydrogenation. Example implementations of this approach in a bifacial design have been presented by Silevo [11] and Tetrasun [24]. An interdigitated back-contact approach has been manufactured by SunPower [112]. For the bifacial structure by Silevo, thin tunnelling oxide layers are capped by graded doped a-Si layers or microcrystalline layers [113]. To fabricate this structure, a comparable process flow to a-Si-based heterojunction solar cells is used, with no evidence of high-temperature processing to enable bulk hydrogenation or gettering on conventional wafer-based silicon solar cells [113]. Similarly, no mention of gettering or bulk hydrogenation has been suggested by Tetrasun, despite mentioning layers that could potentially contain hydrogen and temperatures of more than $600 \, °C$ for film transformation. Laboratory cells using similar approaches of tunnelling oxide and doped polysilicon layers only mention hydrogen passivation in relation to the surface [104]. For SunPower, certain patent embodiments suggest the use of a phosphorus diffusion for FSF formation and PECVD SiN_x, which could enable gettering and hydrogenation of the bulk [114]. However, no discussion of either mechanism was presented. Other work suggests the potential use of tunnel oxide and doped polysilicon layers [115].

A potential cell structure for high-efficiency n-type or p-type devices that could enable bulk hydrogenation and gettering is a hybrid between a homojunction and heterojunction device. Such a structure could take the benefits of conventional processing of phosphorus diffusion, thermal oxidation and PECVD SiN_x:H on the front surface, with a rear surface structure comprised of a heterojunction. With an appropriate processing sequence, the benefits of gettering and bulk hydrogenation could be realised in such a device, while overcoming thermal constraints imposed by the heterojunction structure. For example, if an a-Si heterojunction is used at the rear, the front surface processing could be completed, followed by a firing process for the release of hydrogen from the dielectric layers and bulk defect passivation, before the heterojunction layer is formed. A subsequent low-temperature illuminated hydrogenation process could also be used on the finished device for further bulk defect passivation.

To highlight the compatibility of such a processing sequence with bulk hydrogenation, a test device was fabricated on a p-type mono-crystalline wafer. Half the wafer was passivated on both sides with PECVD SiN_x:H while the other half was masked during the deposition process. A standard co-firing process was used (peak measured sample temperature of $740 \, °C$) to inject hydrogen into the bulk of the wafer in the region coated with SiN_x:H. After firing, the SiN_x:H layer was removed using a 2% HF dip and a fresh surface passivation layer of SiN_x:H was deposited across the entire wafer on both sides (deposition temperature of $\sim 400 \, °C$). It should be noted that the deposition properties of the initial and final SiN_x:H layers were identical and that the deposition process itself does not allow hydrogen to enter the bulk to enable bulk defect passivation [102]. PL images were obtained after the deposition of the fresh SiN_x:H layer, after a 48 h light soak, after a 2 h illuminated hydrogenation process at $200 \, °C$ to passivate boron-oxygen defects, and after a subsequent light-soak to check for stability. The images after the first light soaking process indicated that the sample uniformly degraded prior to the illuminated hydrogenation process (not shown). After the low temperature illuminated hydrogenation process, which is thermally compatible with the use of a-Si-based heterojunction structures ($<250 \, °C$), the calibrated PL iV_{oc} map shown in Fig. 9 highlighted the significant improvement in the hydrogenated regions of the device (top half) by the deliberate injection of hydrogen prior to activating the passivation after the surface passivation layer was applied. Lifetime measurements confirmed that the changes were due to improvements in bulk passivation, rather than surface-related effects.

This demonstrates that effective bulk hydrogenation can be realised for high-efficiency solar cell structures with stringent thermal constraints, by carefully considering opportunities to inject hydrogen into the device, followed by advanced hydrogenation processes after the formation of the device structure.
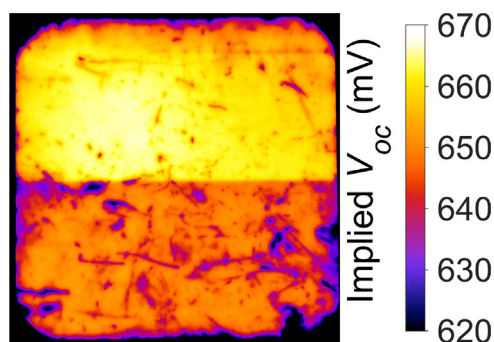
Feature
Article

Phys. Status Solidi A (2017)   (11 of 14) 1700305

Figure 9 Calibrated implied open circuit voltage (V_{oc}) map of a p-type mono-crystalline wafer highlighting the impact of a pre-hydrogenation process applied on the top half of the wafer.

5 Conclusions The role of hydrogenation and gettering were discussed in the context of industrial solar cell fabrication, and the applicability for next-generation solar cells. For p-type solar cells, gettering and hydrogenation naturally occur during the fabrication sequence. However, the transition to the use of lightly doped emitters can reduce the ability to getter impurities such as iron, although the bulk lifetime can simultaneously improve. At the same time, the shift towards a PERC structure can increase the concentration of hydrogen in the bulk, assisting with defect passivation. However, there is evidence to suggest that this could also be a contributing factor to CID in multi-crystalline silicon solar cells. Phosphorus-diffused, screen-printed n-type technologies can similarly benefit from gettering and hydrogenation. For example, Trina has reported a 0.2% absolute efficiency enhancement by gettering impurities to a sacrificial front-surface diffusion in the same process that is required for the formation of the localised BSF regions. However, in general, n-type technologies tend to neglect gettering and bulk hydrogenation. When using alternative metallisation technologies, often high-temperature processing is avoided, particularly when temperature constraints are imposed by the metallisation process. However, this limits the ability to hydrogenate bulk defects. For heterojunction solar cells, the ability to getter the material throughout the fabrication process using conventional methods is removed, and as a result, a deliberate pre-gettering of the wafers may be required. Similarly, the ability to hydrogenate bulk defects is hampered by the use of low-temperature processing and thermal constraints imposed by the heterojunction structures. While this avoids a potential deterioration of the silicon material that can occur during high-temperature processes, it also eliminates the possibility to improve the quality of the silicon throughout the fabrication sequence using hydrogenation. As a result, n-type heterojunction solar cells rely on wafers with high initial bulk lifetimes. To overcome this, high-temperature firing processes can deliberately be performed before metallisation to enable an improved hydrogenation of the bulk. Potentially, homojunction and heterojunction structures can be combined to naturally allow gettering and bulk hydrogenation throughout the fabrication sequence.

References

[1] K. Yoshikawa, "Exceeding Conversion Efficiency of 26% by Silicon Heterojunction Technology," presented at the 7th Silicon PV Conf. April 2017 (2017).

[2] M. A. Green, Prog. Photovolt. Res. Appl. **17**, 183 (2009).

[3] H. Jin, "21.63% world record large area multicrystalline silicon solar cell," oral presentation, ASIA PVSEC Conf. (2016).

[4] X. Wang, Global PV Market (Bloomberg New Energy Finance), oral presentation at the World Solar Congress (2016).

[5] ITRPV Working Group and others, ITRPV Ger. **7**, 29 (2016).

[6] F. Colville, "Understanding the market-share dominance of p-type multi & strategies of leading p-type cell manufacturers," oral presentation, PVCellTech, Kuala Lumpur, 16th March (2016).

[7] ITRPV Working Group and others, ITRPV Ger. **2**, 15 (2011).

[8] H. Fischer and W. Pschunder, in: Proc. 10th IEEE Photovolt. Spec. Conf. (1973), p. 404.

[9] J. E. Cotter, J. H. Guo, P. J. Cousins, M. D. Abbott, F. W. Chen, and K. C. Fisher, IEEE Trans. Electron Devices **53**, 1893 (2006).

[10] O. Schultz-wittmann, D. De Ceuster, A. Turner, D. Crafts, R. Ong, D. Suwito, B. Eggleston, V. Prajapati, A. Kleiman, and K. Bhatt, in: 28th Eur. Photovolt. Sol. Energy Conf. (2013), pp. 1004–1007.

[11] J. B. Heng, J. Fu, B. Kong, Y. Chae, W. Wang, Z. Xie, A. Reddy, K. Lam, C. Beitel, C. Liao, C. Erben, Z. Huang, and Z. Xu, IEEE J. Photovolt. **5**, 82 (2015).

[12] S. Ponce-Alcántara, "Trina Solar sets efficiency record with c-Si cell," PV-Magazine (2015).

[13] C. W. Lan, C. F. Yang, A. Lan, M. Yang, A. Yu, H. P. Hsu, B. Hsu, and C. Hsu, CrystEngComm **18**, 1474 (2016).

[14] H. Li, Average Production Efficiency for P-Type Mono PERC Solar Cells at Lerri Solar (In-House Measurements), private communication (2017).

[15] Trina Solar, "Trina Solar Achieves Average Efficiency of 20.16% for Industrially-Produced Multi-crystalline Silicon PERC Cells and 18.7% for Commercially-Produced Multi-crystalline Silicon DP Cells," (2016). [Online]. Available: <www.trinasolar.com/us/news/trina-solar-achieves-average-efficiency-2016-industrially-produced-multi-crystalline-silicon>.

[16] I. Clover, "REC achieves +20% efficiency for mass production of multicrystalline solar cells," (2016). [Online]. Available: <www.pv-magazine.com/2016/10/05/rec-achi eves-20-efficiency-for-mass-production-of-multicrystalline -solar-cells_100026368/>.

[17] Trina Solar, "Trina Solar Announces Achievement of 21.1% Average Efficiency for Industrially-Produced Monocrystalline PERC Cells," (2016). [Online]. Available: <www.trinasolar.com/us/news/trina-solar-announces-achi evement-211-average-efficiency-industrially-produced-monocrystalline>.

[18] F. Fertig, "Mass Production of p-Type Cz Silicon Solar Cells Approaching Average Stable Conversion Efficiencies of 22 %," presented at the 7th Silicon PV Conf. April 2017 (2017).

[19] M. Hutchins, "Suntech announces 20% efficiency for mass-production multi-PERC cell," (2017). [Online]. Available: <www.pv-magazine.com/2017/01/11/suntech-announces-20-efficiency-for-mass-production-multicrystalline-perc-cell/>.

[20] LG Electronics, "LG Solar − Tomorrow's high-efficiency PV technology, available today," (2013). [Online]. Available: <www.lgenergy.co.nz/uploads/download_files/9f4a 25e966a5f55e52ee732d57a790d207d83a8d.pdf>.

[21] J. Shi, Sol. Energy **142**, 87 (2016).

[22] Kaneka, "World's Highest Conversion Efficiency of 26.33% Achieved in a Crystalline Silicon Solar Cell," (2016). [Online]. Available: <www.kaneka.co.jp/kaneka-e/ images/topics/1473811995/1473811995_101.pdf>.

[23] K. Masuko, M. Shigematsu, T. Hashiguchi, D. Fujishima, M. Kai, N. Yoshimura, T. Yamaguchi, Y. Ichihashi, T. Mishima, N. Matsubara, T. Yamanishi, T. Takahama, M. Taguchi, E. Maruyama, and S. Okamoto, IEEE J. Photovolt. **4**, 1433 (2014).

[24] O. Schultz-wittmann, A. Turner, B. Eggleston, D. De Ceuster, D. Suwito, E. Van, S. Baker-finch, and V. Prajapati, in: Proc. 32nd Eur. Photovolt. Sol. Energy Conf. (2016), pp. 456–459.

[25] M. Osborne, "SunPower makes major module technology shift on 2GW production target," PVTech (2015). [Online]. Available: <www.pv-tech.org/news/sunpower-makes-maj or-module-technology-shift-on-2gw-production-target>.

[26] B. Sopori, J. Electron. Mater. **31**, 972 (2002).

[27] A. Bentzen and A. Holt, J. Appl. Phys. **99**, 1 (2006).

[28] A. G. Aberle, Sol. Energy Mater. Sol. Cells **65**, 239 (2001).

[29] J. Chen, D. Yang, Z. Xi, and T. Sekiguchi, Physica B Condens. Matter **364**, 162 (2005).

[30] M. Sheoran, A. Upadhyaya, and A. Rohatgi, Solid State Electron. **52**, 612 (2008).

[31] B. Hallam, A. Sugianto, L. Mai, G. Xu, C. Chan, M. Abbott, S. Wenham, A. Uruena, E. Cornagliotti, and M. Aleman, IEEE J. Photovolt. **4**, 1413 (2014).

[32] B. J. Hallam, C. E. Chan, M. D. Abbott, and S. R. Wenham, Sol. Energy Mater. Sol. Cells **141**, 125 (2015).

[33] K. Münzer, in: Proc. 24th Eur. Photovolt. Sol. Energy Conf. Hambg. (2009), pp. 1558–1561.

[34] J. Schmidt, B. Lim, D. Walter, K. Bothe, S. Gatz, T. Dullweber, and P. P. Altermatt, IEEE J. Photovolt. **3**, 114 (2013).

[35] E. Letty, "On the Defect Responsible for the Carrier Injection-induced Degradation of Uncompensated n-Type Czochralski Silicon," presented at the 7th Silicon PV Conf. April 2017.

[36] D. D. Smith, P. J. Cousins, A. Masad, A. Waldhauer, S. Westerberg, M. Johnson, X. Tu, T. Dennis, G. Harley, G. Solomon, S. Rim, M. Shepherd, S. Harrington, M. Defensor, A. Leygo, P. Tomada, J. Wu, T. Pass, L. Ann, L. Smith, N. Bergstrom, C. Nicdao, P. Tipones, and D. Vicente, in: Proc. 38th IEEE Photovolt. Spec. Conf. (2012), pp. 1594–1597.

[37] D. Sperber and A. Herguth, Energy Proc. **92**, 211 (2016).

[38] M. Taguchi, A. Terakawa, E. Maruyama, and M. Tanaka, Prog. Photovolt. Res. Appl. **13**, 481 (2005).

[39] J. Chen and T. Sekiguchi, Jpn. J. Appl. Phys. **46**, 6489 (2007).

[40] A. Cuevas, D. MacDonald, M. Kerr, C. Samundsett, A. Sloan, S. Shea, A. Leo, M. Mrcarica, and S. Winderbaum, in: Conf. Rec. 28th IEEE Photovolt. Spec. Conf. (2000), pp. 244–247.

[41] V. Vähänissi, A. Haarahiltunen, H. Talvitie, M. Yli-Koski, and H. Savin, Prog. Photovolt. Res. Appl. **21**, 1127 (2013).

[42] S. Ponce-Alcántara, C. Del Cañizo, and A. Luque, Sol. Energy Mater. Sol. Cells **87**, 411 (2005).

[43] A. Ourmazd and W. Schröter, Appl. Phys. Lett. **45**, 781 (1984).

[44] H. Wagner, A. Dastgheib-Shirazi, B. Min, A. E. Morishige, M. Steyer, G. Hahn, C. Del Cañizo, T. Buonassisi, and P. P. Altermatt, J. Appl. Phys. **119**, 185704 (2016).

[45] D. Abdelbarey, V. Kveder, W. Schröter, and M. Seibt, Appl. Phys. Lett. **94**, 061912 (2009).

[46] L. A. Verhoef, P. Michiels, S. Roorda, W. C. Sinke, and R. J. C. Van Zolingen, Mater. Sci. Eng. B **7**, 49 (1990).

[47] M. Apel, I. Hanke, R. Schindler, and W. Schröter, J. Appl. Phys. **76**, 4432 (1994).

[48] D. Macdonald, A. Y. Liu, and S. P. Phang, Solid State Phenomena. **205–206**, 26–33 (2013).

[49] D. Macdonald, A. Cheung, and A. Cuevas, in: 3rd World Conf. on Photovolt. Energy Conversion (2003), pp. 11–14.

[50] B. Michl, J. Schön, W. Warta, and M. C. Schubert, IEEE J. Photovolt. **3**, 635 (2013).

[51] A. E. Morishige, H. S. Laine, J. Schön, A. Haarahiltunen, J. Hofstetter, C. del Cañizo, M. C. Schubert, H. Savin, and T. Buonassisi, Appl. Phys. A Mater. Sci. Process. **120**, 1357 (2015).

[52] J. F. Lelièvre, J. Hofstetter, A. Peral, I. Hoces, F. Recart, and C. del Cañizo, Energy Proc. **8**, 257 (2011).

[53] R. A. Sinton, A. Cuevas, and M. Stuckings, in: Proc. 25th IEEE Photovolt. Spec. Conf. (1996), pp. 457–460.

[54] H. Nagel, C. Berge, and A. G. Aberle, J. Appl. Phys. **86**, 6218 (1999).

[55] D. H. Macdonald, L. J. Geerligs, and A. Azzizi, J. Appl. Phys. **95**, 1021 (2004).

[56] C. Herring, N. M. Johnson, and C. G. de Walle, Phys. Rev. B **64**, 125209 (2001).

[57] D. Mathiot, Phys. Rev. B **40**, 5867 (1989).

[58] C.-T. Sah, R. N. Noyce, and W. Shockley, Proc. IRE **45**, 1228 (1957).

[59] C. Sun, F. E. Rougieux, and D. Macdonald, J. Appl. Phys. **117**, 45702 (2015).

[60] F. Jiang, M. Stavola, A. Rohatgi, D. Kim, J. Holt, H. Atwater, and J. Kalejs, Appl. Phys. Lett. **83**, 931 (2003).

[61] P. Hamer, B. Hallam, C. Chan, A. Wenham, A. Sugianto, M. Abbott, and S. Wenham, in: Proc. 28th Eur. Photovolt. Sol. Energy Conf. Paris, France (2013), pp. 982–987.

[62] B. Hallam, B. Tjahjono, T. Trupke, and S. Wenham, J. Appl. Phys. 115, 44901 (2014).

[63] T. Trupke, R. A. Bardos, M. C. Schubert, and W. Warta, Appl. Phys. Lett. 89, 44107 (2006).

[64] A. Teal and M. Juhl, in: 2015 IEEE 42nd Photovolt. Spec. Conf. (PVSC 2015).

[65] D. Payne, C. Castrillon, Z. Hameiri, S. Wenham, and D. Bagnall, Comput. Phys. Commun. 215, 223 (2017).

[66] B. J. Hallam, P. G. Hamer, S. Wang, L. Song, N. Nampalli, M. D. Abbott, C. E. Chan, D. Lu, A. M. Wenham, L. Mai, N. Borojevic, A Li, D. Chen, M. Y. Kim, A. Azmi, and S. Wenham, Energy Proc. 77, 799 (2015).

[67] B. Hallam, C. Chan, D. N. R. Payne, D. Lausch, M. Gläser, M. Abbott, and S. Wenham, Photovolt. Int. 33, 37 (2016).

[68] L. Song, A. Wenham, S. Wang, P. Hamer, A. Shakil, B. Hallam, L. Mai, M. Abbott, E. Hawkes, C. Chong, and S. Wenham, Int. J. Photoenergy 501, 193892 (2015).

[69] A. F. Carroll, 2013 IEEE 39th Photovolt. Spec. Conf. (PVSC 2013), p. 3435.

[70] T. Lauermann, A. Dastgheib-Shirazi, F. Book, B. Raabe, G. Hahn, H. Haverkamp, D. Habermann, C. Demberger, and C. Schmid, Proc. 24th Eur. Photovolt. Sol. Energy Conf. Hambg. (2009).

[71] R. Dumbrell, P. Hamer, A. Lennon, and B. Tjahjono, Proc. 2010 Aust. Sol. Energy Soc. Conf., Canberra, Australia (2010), p. 131.

[72] H. Hannebauer, T. Dullweber, S. Wyczanowski, K. Weise, F. Delahaye, O. Doll, I. Köhler, and R. Brendel, in: 28th Eur. Photovolt. Sol. Energy Conf. (2013), pp. 752–756.

[73] Z. Wang, P. Han, H. Lu, H. Qian, L. Chen, Q. Meng, N. Tang, F. Gao, Y. Jia, J. Wu, W. Wu, H. Zhu, J. Ji, Z. Shi, A. Sugianto, L. Mai, B. Hallam, and S. Wenham, Prog. Photovolt. Res. Appl. 20, 260 (2012).

[74] A. G. Aberle, Prog. Photovolt. Res. Appl. 8, 473 (2000).

[75] J. Zhao, A. Wang, P. P. Altermatt, S. R. Wenham, and M. A. Green, Sol. Energy Mater. Sol. Cells 41, 87 (1996).

[76] S. Mack, U. Jäger, G. Kastner, E. A. Wotke, U. Belledin, A. Wolf, R. Preu, and D. Biro, Proc. 35th IEEE Photovolt. Spec. Conf. (2010), p. 34.

[77] A. Wolf, S. Mack, C. Brosinsky, M. Hofmann, P. Saint-Cast, and D. Biro, Conf. Rec. IEEE Photovolt. Spec. Conf. (2011), p. 3568.

[78] A. Richter, S. W. Glunz, F. Werner, J. Schmidt, and A. Cuevas, Phys. Rev. B 86, 165202 (2012).

[79] A. Cuevas and D. Macdonald, Sol. Energy 76, 255 (2004).

[80] S. Wilking, J. Engelhardt, S. Ebert, C. Beckh, A. Herguth, and G. Hahn, 29th Eur. Photovolt. Sol. Energy Conf. Exhib. (2014), p. 366.

[81] B. J. Hallam, M. Abbott, N. Nampalli, P. G. Hamer, and S. R. Wenham, IEEE J. Photovolt. 6, 92 (2015).

[82] B. Hallam, M. Abbott, N. Nampalli, P. Hamer, and S. Wenham, J. Appl. Phys. 119, 65701 (2016).

[83] V. P. Markevich, M. V. Contreras, J. Mullins, M. Halsall, B. Hamilton, L. I. Murin, R. Falster, J. Binns, E. Good, J. Coutinho, J. Medford, C. L. Reynolds Jr, and A. R. Peaker, Proc. 43rd IEEE PVSC (2016), p. 688.

[84] K. Ramspeck, S. Zimmermann, H. Nagel, A. Metz, Y. Gassenbauer, B. Birkmann, and A. Seidl, Proc. 27th Eur. Photovolt. Sol. Energy Conf. Frankfurt/Main, Germany (2012), p. 861.

[85] F. Kersten, J. Heitmann, and J. Müller, 32nd Eur. Photovolt. Sol. Energy Conf. Exhib. (2016), p. 507.

[86] K. Nakayashiki, J. Hofstetter, A. E. Morishige, T.-T. A. Li, D. B. Needleman, M. A. Jensen, and T. Buonassisi, IEEE J. Photovolt. 6, 860 (2016).

[87] S. Frigge, H. Mehlich, and T. Grosse, 31st Eur. Photovolt. Sol. Energy Conf. 5AV.6.4 (2015).

[88] C. E. Chan, D. N. R. Payne, B. J. Hallam, M. D. Abbott, T. H. Fung, A. M. Wenham, B. Tjahjono, and S. R. Wenham, IEEE J. Photovolt. 6, 1473 (2016).

[89] D. Bredemeier, D. Walter, S. Herlufsen, and J. Schmidt, AIP Adv. 6, 35119 (2016).

[90] R. Eberle, W. Kwapil, F. Schindler, M. C. Schubert, and S. W. Glunz, Phys. Status Solidi RRL 5, 1 (2016).

[91] C. Chan, T. H. Fung, M. Abbott, D. Payne, A. Wenham, B. Hallam, R. Chen, and S. Wenham, Sol. RRL 1, 1600028 (2017).

[92] P. J. Cousins, D. D. Smith, H.-C. Luan, J. Manning, T. D. Dennis, A. Waldhauer, K. E. Wilson, G. Harley, and W. P. Mulligan, in: Proc. 35th IEEE Photovolt. Spec. Conf. (2010), pp. 275–278.

[93] W. P. Mulligan, M. J. Cudzinovic, T. Pass, D. Smith, N. Kaminar, K. McIntosh, and R. M. Swanson, Solar Cell and Method of Manufacture, Patent US7897867 (2008).

[94] W. P. Mulligan, M. J. Cudzinovic, T. Pass, D. Smith, and R. M. Swanson, Metal Contact Structure for Solar Cell and Method of Manufacture, Patent US7388147 (2008).

[95] M. Taguchi, K. Kawamoto, S. Tsuge, T. Baba, H. Sakata, M. Morizane, K. Uchihashi, N. Nakamura, S. Kiyama, and O. Oota, Prog. Photovolt. 8, 503 (2000).

[96] A. B. Turner, O. Schultz-Wuttnann, D. De Ceuster, and D. E. Crafts, Selective Transformation in Functional Films, and Solar Cell Applications Thereof, Patent US20120186649 (2010).

[97] Z. Li, Y. Yang, X. Zhang, W. Liu, Y. Chen, G. Xu, X. Shu, Y. Chen, P. P. Altermatt, Z. Feng, and P. J. Verlinden, in: Proc. 32nd Eur. Photovolt. Sol. Energy Conf. (2016), pp. 571–574.

[98] D. Lecrosnier, J. Paugam, G. Pelous, F. Richou, and M. Salvi, J. Appl. Phys. 52, 5090 (1981).

[99] V. Vähänissi, A. Haarahiltunen, M. Yli-koski, and H. Savin, IEEE J. Photovolt. 4, 142 (2014).

[100] M. Aleman, A. de Castro, P. Choulat, B. Hallam, C. Dang, R. Russell, F. Duerinckx, E. Cornagliotti, and J. Szlufcik, in: 29th Eur. Photovolt. Sol. Energy Conf., Amsterdam (2014), pp. 528–531.

[101] J. Hong, W. M. M. Kessels, W. J. Soppe, A. W. Weeber, W. M. Arnoldbik, and M. C. M. de Sanden, J. Vac. Sci. Technol. B Microelectron. Nanom. Struct. 21, 2123 (2003).

[102] N. Nampalli, B. J. Hallam, C. E. Chan, M. D. Abbott, and S. R. Wenham, IEEE J. Photovolt. 5, 1580 (2015).

[103] B. Hallam, High Efficiency Laser-Doped Silicon Solar Cells with Advanced Hydrogenation, PhD thesis, University of New South Wales, Australia (2014).

[104] S. W. Glunz, F. Feldmann, A. Richter, M. Bivour, C. Reichel, H. Steinkemper, J. Benick, and M. Hermle, in: Proc. 31st Eur. Photovolt. Sol. Energy Conf. Exibition (2015), pp. 259–263.

[105] R. J. Falster, D. Gambaro, M. Cornara, M. Olmo, and M. Pagani, Solid State Phenom. 57, 123 (1997).

[106] S. R. Wenham, P. G. Hamer, B. J. Hallam, A. Sugianto, C. E. Chan, L. Song, P. H. Lu, A. M. Wenham, L. Mai, C. M. Chong, G. X. Xu, and M. B. Edwards, Advanced Hydrogenation of Silicon Solar Cells, Patent US 9190556 B2 (2015).

[107] A. Urueña, M. Aleman, E. Cornagliotti, A. Sharma, M. Haslinger, L. Tous, R. Russell, J. John, F. Duerinckx, and J. Szlufcik, Prog. Photovolt. Res. Appl. 24, 1149 (2016).

[108] M. Tanaka, S. Okamoto, S. Tsuge, and S. Kiyama, 2003. Proc. 3rd World Conf. Photovolt. Energy Conversion (2003).

[109] K. R. McIntosh and P. P. Altermatt, in: Proc. 35th IEEE Photovolt. Spec. Conf. (2010), pp. 2188–2193.

[110] A. Y. Liu, C. Sun, V. P. Markevich, A. R. Peaker, J. D. Murphy, and D. Macdonald, J. Appl. Phys. 120, 193103 (2016).

[111] R. A. Street, Hydrogenated Amorphous Silicon (Cambridge University Press, Cambridge, UK, 1991).

[112] D. D. Smith, P. J. Cousins, A. Masad, S. Westerberg, M. Defensor, T. Dennis, R. Daquin, N. Bergstrom, A. Leygo, X. Zhu, B. Meyers, M. Shields, and D. Rose, in: Proc. 39th IEEE Photovolt. Spec. Conf. (2013), pp. 908–913.

[113] J. B. Heng, C. Yu, Z. Xu, and J. Fu, Solar Cell with Oxide Tunneling Junctions, Patent US8686283 (2014).

[114] D. Smith, Backside Contact Solar Cell with Formed Polysilicon Doped Regions, Patent US8647911 (2012).

[115] R. Swanson, Back Side Contact Solar Cell with Doped Polysilicon Regions, Patent US7633006 (2009).